Understanding ground deformation mechanisms for multi-propped excavation in soft clay

Lam, S.Y., S.K. Haigh and Bolton, M.D.

University of Cambridge

Abstract

Many deep excavation works have been carried out to construct various types of underground infrastructure such as deep basements, subways and service tunnels. The execution of these deep excavation works requires the use of appropriate retaining wall and bracing systems. Inadequate support systems have always a major concern, as any excessive ground movement induced during excavation could cause damage to neighboring structures, resulting in delays, disputes and cost overruns. To gain a better understanding on the mechanisms involved in soil excavation, centrifuge model tests of deep excavations in slightly over-consolidated soft clay have been carried out using a newly developed testing system, in which the construction sequence of a multi-propped wall for deep excavation can be properly simulated in flight. Deformation mechanisms are observed using Particle Image Velocimetry. Settlements of the ground surface and changes in pore water pressure are monitored during excavation. The effect of different props stiffness, wall rigidity and excavation geometry on the characteristics of ground deformation and soil-structure interaction were demonstrated and discussed. Conservation of energy as a principle for the mobilizable strength design method for calculating ground movement was validated and performed satisfactorily.

Introduction

To better understanding on the mechanisms involved in soil excavation, centrifuge model tests of deep excavations in slightly over-consolidated soft clay have been carried out using a newly developed testing system, in which the construction sequence of a multi-propped wall for deep excavation can be properly simulated in flight.

Methodology

Small-scale centrifuge models can been used to simulate the prototype behavior of an excavation

in soil. A centrifugal acceleration field is used in a small scale model to match the stresses induced by gravity in the prototype. The principal challenges are to design a test package to simulate the construction sequence of a braced excavation in the field, so that a cross-section can be used for the remote measurement of resulting ground movements. The advantage is that tests can be repeated with planned variations, and that the model can be observed continuously from the occurrence of small deformations up to complete collapse, which is not generally allowed to happen in the field.

Test programme

Five centrifuge model tests were carried out to study the undrained short-term behaviour of excavation in soft clays. Test 1 investigated the behaviour of a floating rigid wall supported by stiff props. It acted as a reference test for comparisons. Test 2 studied the effect of wall flexibility on the deformation mechanism. Test 3 looked into the problem of using a base slab to modelling a grout layer to fix the wall toe movement in bending and shear mode. Test 4 simulated a rigid wall supported by soft props to study the effect of soft propping on the changes in deformation pattern. Test 5 studied a case of excavation in shallow clay using flexible wall. A summary of the test programme is given in Table 1.

Table 1 A summary of centrifuge testing programme

Centrifuge Tests	1	2	3	4	5
Objectives	Floating Rigid wall with stiff props Baseline test	Floating Flexible wall with stiff props Wall stiffness	Fixed base Flexible wall with base grout Fixed wall toe condition	Floating Rigid wall with soft props Prop stiffness	Fixed base Flexible wall in shallow clay Clay thickness
D (mm) in model scale	300	300	300	300	160
Prop stiffness (kN/mm) in model scale	1.66	1.66	1.66	0.55	1.66
System stiffness $EI/\gamma_w s^4$	2860	106	106	2860	106
Toe fixity	Free	Free	Fixed	Free	Free

Experimental setup

Figure 1 shows the experimental setup of the present study. The rectangular model container is made of aluminum alloy with internal dimensions 790mm in length, 180mm in width and 470mm

in depth. The front face of the container consists of a Perspex window, which enables the whole testing process to be monitored by cameras mounted in front. The back of the container has holes at specific locations with respect to the position of the retaining wall, for installation of pore pressure transducers and the provision of drainage.

A new two-axis servo actuator was designed for the Turner Beam Centrifuge at Cambridge University (Lam et al., 2012). The actuator can apply a maximum load of 10kN in analogue vertical and horizontal directions, with a maximum speed of 5mm/s, at an in-flight acceleration up to 100g. The servo actuator stands above the rim of the model container. The carrier plate of the actuator is connected through a screw fitting to an inverted T-shaped scraper which performs in-flight excavation at 60g.

Instrumentation comprising pore pressure transducers in the soil, earth pressure cells on the retaining wall, bending moment strain gauges on the wall, load cells on the props and linear variable transformers for displacement measurements were installed. Digital cameras were mounted in front of the Perspex window and LED arrays were situated to illuminate the clay cross-section without causing glare, or shadows.

The vertical plane through the center of an excavation can be regarded as a plane of symmetry. A "gate wall" (as shown in Figure 1) aims to represent this plane of symmetry, so that only one side of the excavation needs be modeled. PTFE sheets were glued on the gate wall to minimize vertical friction, and steps are also taken to prevent its lateral movement prior to excavation. A prop installation sub-system was designed to provide in-flight support, initially to the gate wall and ultimately to the retaining wall, during the experiment. Three pairs of cylinders (Festo DSNU 25-125) are mounted on a rigid support frame and positioned at 0 mm, 36 mm and 72 mm below the initial clay surface. Props are driven via pistons in the cylinders which are actuated through a hydraulic/pneumatic control system. Backward pressure inlets are connected to a compressed air source for retreating the cylinders. Forward pressure inlets are connected to an oil pressure reservoir so that they can provide a similar propping force at each excavation level. Each level of props is controlled individually through solenoid valves. The oil supply manifold is connected to an air-oil interface through a needle valve which is used to control the rate of advance of each pair of props, in sequence. Compressed air acting on the front face of the pistons is transmitted from an external compressor and regulator, and is supplied to the centrifuge through a pneumatic coupling.

Before the experiment, the system is saturated with hydraulic oil. The prop stiffness is obtained by conducting axial-load displacement tests in a loading rig. The target stiffness of a fully-saturated prop is found to be about 1.66kN/mm. Figure 2 shows the gate system. At the start of the experiment, three pairs of sacrificial gates, each 36mm high, sit on the top of the gate wall. They act as a support to retain the soil to be excavated. The gates are temporarily supported by the pairs of cylinders throughout the initial reconsolidation stage before excavation. The forces required to support the gate segments are monitored by axial load cells attached at the end of each prop. Figure 2 shows the sequence of the first excavation stage. At the start of excavation, the first pair of cylinders is retracted so that the first layer of gates is in an unstable condition and is easily knocked down by the scraper of the in-flight excavator. The in-flight excavator then makes a 4 mm cut into the soil, which is scraped off into the open space inside the cylinder support system. The scraper then returns to its initial position and makes another 4 mm cut, repeating until the excavation level reaches the top of the second level of gates. At that moment, the first level of props is pressurized again to support the retaining wall. The prop force required can be adjusted by looking at the readings given by the prop load cells. This completes the first stage of excavation. As the scraper is specially made in an inverted T-shape, it can continue scraping below the first pair of props. The second and third stages of excavation can therefore proceed by repeating the same steps carried out for the first level.

Model making and instrumentations

Standardization of experimental procedures is very important as it determines the ability to reproduce similar soil stress states in each experiment. Both clay and sand were used in the present experiments.

A base layer of fine Fraction E sand was formed by pluviation using an automatic pouring machine (Madabhushi *et al*., 2006; Zhao *et al*, 2006). A constant fall-height of 600 mm was used to achieve a uniform layer with a relative density above 95% and a dry unit weight of 16.0 kN/m^3. The properties of the sand are shown in Table 2. Saturation of the sand was effected by connecting the bottom drainage hole to a standpipe filled with water.

Since the objective of these particular tests was to monitor excavation in soft clay and to compare different bracing schemes, lightly over-consolidated kaolin clay was used in the models. A standard procedure was adopted to ensure repetitive reproduction of the model ground with similar

strength profiles in each test. Speswhite kaolin clay was chosen for the tests because the parameters are well defined in the literature: some mineralogy and properties are given Table 3. Clay powder was mixed with water to about twice the liquid limit (i.e. 120% moisture content), the mixing taking place under vacuum for at least two hours. The inner surface of the test container was coated with silicone grease to minimize friction against the clay. The clay slurry was carefully poured on the bearing layer, which consisted of a sheet of filter material placed over the base layer of sand. The final height of the slurry was 550mm. The container was placed in a hydraulic press, and pressure was applied to the clay in six loading steps (to 2 kPa, 5 kPa, 10 kPa, 20 kPa, 40 kPa and 80 kPa, and 160 kPa). The final pressure of 160 kPa was intended to achieve an estimated c_u of 25 kPa for the clay at mid-depth in the centrifuge model when it had swollen back into equilibrium at 60 g.

When the settlement of the clay in the press became steady under 80 kPa, the clay was unloaded. Nine PPTs were inserted through pre-drilled openings in the back wall of the container. PPTs were installed through 90 mm long holes augured horizontally into the clay using a hand drill. Unconsolidated slurry was then injected to fill the holes, and the openings were sealed. The final locations of the PPTs are shown in Figure 3. The spacing between PPTs was about 30mm. After installation, loading was brought back to 80kPa. After equilibration, the consolidation pressure was further increased to 160kPa. After settlement was steady, the pressure was reduced again to 80 kPa and the clay was allowed to swell into equilibrium. Removal of this final pressure was known to be possible without drawing air into the clay.

The loading plate was removed. After trimming the clay surface, the resulting clay thickness was 295mm. The front wall of the model container was then removed. The clay and base layer were then removed from that half of the package that would contain the cylinder support system. An O-ring seal was placed along the edges of the gate wall to seal the gap at the side walls of the box. The retaining wall, in the particular test to be described here, is made of either a 2mm or a 6mm thick aluminum alloy plate with an equivalent stiffness (EI) of 10.4 MNm/m^2 or 280.8 MNm/m^2 at prototype scale, respectively. These walls simulate a sheet pile wall (US steel, PDA-27) and a 0.9m thick diaphragm wall in the field.

Aluminium alloy was chosen as it is stiff and light. This reduces the effect of excessive settlement of the wall in soft ground during self-weight consolidation. Greased wiper seals were used to

prevent water from seeping past the sides of the wall and to ensure a free sliding condition with minimal friction. The wall was installed at a depth of 160 mm (equivalent to 10.6 m prototype). A set of vertical guides and a cutter were used to dig a trench with the same thickness as the wall. The wall was then pushed into the trench using a vertical guide.

With the clay cross-section uppermost, grains of black-dyed fraction E sand were blown onto the clay to provide PIV texture. Lubricant was then applied to the Perspex window to reduce friction against the soil cross-section. The hollow frame, Perspex window and window frame were then bolted to the main body of the container.

LVDTs were assembled at 30 mm spacing intervals from the wall to measure the soil settlement profile. A laser sensor was used to monitor the lateral displacement of the top of the wall. Finally, the water table in the clay was to be maintained at the ground surface by permitting overflow from a stand pipe which would be supplied continuously throughout the experiment. Two 8 megapixels cameras took pictures throughout the experiment with the provision of suitable lighting. The detailed locations of the instrumentation are shown in Figure 3.

Undrained strength profile and stress strain curves at small strain

Consolidated triaxial compression tests were carried out to characterize undrained shear strength of the soil. The undrained shear strength was found to be 22.5kPa as shown in Figure 4. In the same figure, an estimated profile an empirical relation suggested by Jamiolkowski et al.(1985), respectively, was also shown for comparisons.

Jamiolkowski et al. (1985) related the c_u of the soil with the vertical effective stress of the soil and undrained strength ratio for normally consolidated clay and over-consolidation ratio. The empirical correlation is defined as follows:

$$c_u = 0.22\sigma_v'(OCR)^{0.8} \quad (1)$$

In the present studies, the stress strain behaviour of light over-consolidated Speswhite kaolinite at small and intermediate strain levels were studied using a new local strain measurement and dynamic wave propagation system incorporated into a triaxial apparatus. Only isotropically consolidated compression test were carried out on vertically- and horizontally cut 100mm by 50mm cylindrical specimens. The local deformation data of four specimens was obtained from undrained compression tests on blocky soil samples pre-consolidated at 160 kPa. The deformation

data from the local LVDTs on the specimens were logged into a computer along with other triaxial data. The secant young's modulus was then calculated as a ratio of the deviator stress and locally measured axial strain. Subsequently, the undrained shear modulus was derived by assuming a poisson ratio of 0.5. The secant axial modulus was plotted against local strain on a semi-log scale for the purpose of investigating the stiffness degradation for very small to finite strain range. All specimens were initially isotropically consolidated to 125 kPa and then allowed to swell back to 26kPa before application of compressive load to replicate the mean stress at mid depth of the wall. Then, compressive load was applied within 8 hours at a rate of 0.16mm/hr. As observed in the stress-strain curves and the stiffness degradation curve as shown in Figure 5, the horizontally cut specimen is mildly stiffer and stronger than the vertically-cut specimens. This could be ascribed to the direction of the bedding plane of clay particles formation during the deposition and one-dimensional consolidation.

Geophysical soil characterization technique, bender element test, is utilized to obtain the shear wave velocity. By sending shear waves with a high frequency of 1kHz, the difference between the arrival time and input signal is assessed by cross-correlation method. The sample length to wavelength ratio is chosen to be 9.6 in order to separate the near field coupled compression and shear waves avoiding near-field effect (Leong et al., 2005).

From the shear wave velocity, the shear stiffness G_{max} can be determined from the elastic wave propagation theory:

$$G_{\max} = \rho V_s^{\,2} \tag{2}$$

where ρ is the total density of the soil specimen.

Three bender element tests have been carried out on a vertical and two horizontal core samples. The maximum shear G_{max} of the vertical and horizontal cored samples are found to be about 16MPa and 18MPa, respectively.

The current test results at very low confining stress were plotted together with Viggiani and Atkinson (1995) with medium confining stress in a logarithmic G_o/p_r and p'/p_r space Figure 6(a), where p_r is a reference pressure taken to be 1 kPa. The data point on the plot fell close to a single straight line given in Equation 3:

$$\frac{G_o}{p_r} = A\left(\frac{p'}{p_r}\right)^n \left(\frac{p_{\max}}{p'}\right)^m \quad (3)$$

,where A and n are non-dimensional soil parameters. The parameters A, n and m are found to be 2088, 0.653 and 0.194, respectively. The coefficient of correlation r^2=0.82 was obtained. For the present study, the calculated G_o by applying the empirical Equation (3) was found to be 22MPa. The measured values obtained from bender element tests of the present study were within 20% of the prediction.

A hyperbolic function is introduced to relate secant shear modulus with G_o, shear strain γ and the reference strain $\gamma_{ref.}$ Reference strain γ_{ref} was assumed to be a linear function of void ratio following Vardanega (2012).

Using the least square method, the coefficient of correlation was found to be 0.82. The parameters *a* and *b* in Equation 4 and 5 were found to be 0.69 and 2.3, respectively. The correlation is plotted together with the actual measurement for comparison in Figure 6(b).

$$\frac{G}{G_o} = \frac{1}{1+\left[\frac{\gamma}{\gamma_{ref}}\right]^a} \quad (4)$$

$$\gamma_{ref} = be_o \times 10^{-3} \quad (5)$$

Excavation test procedures

The in-flight excavator was bolted above the model container, and the integrated assembly was transferred onto the centrifuge swing platform. This was fixed to the torsion-bar catches which permit the package to rotate into a fixed-end condition at a centrifuge acceleration of about 10 g. The model was then brought to its scale acceleration of 60g. There are three test phases for a typical centrifuge test of deep excavation – reconsolidation, in-flight excavation, and long-term equilibration.

As an increase in soil self-weight leads to an increase in excess pore pressure, the model ground first had to undergo about 5 hours of reconsolidation until at least 90% of the consequential consolidation was achieved. The degree of consolidation was monitored by judging whether pore pressure transducer (PPT) readings were approaching their hydrostatic state.

The excavation was then started. The in-flight excavator operated at a rate of 10 mm/s horizontally and with 4 mm vertical increments. In order to ensure that realistic quasi-undrained responses were observed, the excavation process should be finished within a reasonably short period of time. Figure 7 shows the progress of excavation in all tests. Excavation to an excavation depth of 5.5 m finished within 30-40 minutes (72-96 days at prototype scale), which is similar to the rate of excavation in the field.

Following excavation, the test was allowed to continue and excess pore pressures that had been generated by excavation were observed to dissipate as long term deformations were monitored. In the following section, only ground deformation data of the tests are presented.

Typical pore pressure responses

As the excavation proceeds, the ground water level in front of the wall was lowered simultaneously. The bottom drainage layer was connected to a standpipe which maintains a hydrostatic water pressure measured from soil surface at the back of the wall throughout each test. Water flow through the sides of the wall was prevented by greased seals. Under such condition, downward seepage at the backside of the wall and upward seepage in front of the wall should be expected. Figure 8 shows the variation of pore water pressure during excavation using a 0.9m thick diaphragm wall in Test 1. In front of the wall, there was a negative pore pressure built-up (PPT 9 and PPT 8) due to the reduction in total mean stresses during excavation. The magnitude of the negative pore pressures was smaller than the effective over-burden pressure lost in excavation. This is owing to the fact that the negative pore pressure were cancelled out by the positive pore pressures generated by shear deformation of clay. On the other hand, the change in pore pressure measured at the back of the retaining wall (PPT 1, PPT 2 and PPT 3) was relatively small because the stiff prop supports limited lateral wall deformation and thus limited reduction in lateral horizontal stress.

Ground settlement and wall deflection

The characteristics of wall deflection and ground settlement profile during undrained excavation is a vital parameter for assessing potential damages to neighboring structures and buried services. In an ideal excavation process, the support level is installed at an early stage in order to minimize cantilever movement of the wall. However, this may not be always possible in practice due to a variety of site constraints and construction sequences. In the present studies, the excavation

procedures initiated with a cantilever stage of excavation, which was then followed by singly propped and finally multi-propped excavation. Ground movements were captured by the PIV technique. Results of ground settlement profile at some discrete measurement point away from the retaining wall monitored by LVDTs are also included for comparisons for Test 2. In general, the results obtained by LVDTs and the PIV technique are comparable, which ensures that the model is testing under plane strain condition properly.

Figure 9 shows the development of lateral wall displacement and ground settlement of a deep excavation using flexible wall (Test 2). Consistent with results shown by previous researchers (Powrie, 1986), rotation of wall about the wall toe was observed in the cantilever excavation stage. Maximum incremental cantilever wall deflection of about 10mm (Figure 9(a)) was observed at the wall crest in prototype scale(0.167mm in model scale), which is equivalent to 0.2% of average engineering shear strain in the 45 degree triangular zone behind the wall according to Osman and Bolton (2004).

Considering the incremental deformations of a multi-propped wall supporting a deep excavation in soft, undrained clay, at each stage of excavation the incremental displacement profile of the ground and the wall below the lowest prop was assumed to be a cosine function by O'Rourke(1993) as shown in Figure 13.

$$\delta w = \frac{\delta w_{\max}}{2}\left(1-\cos(\frac{2\pi y}{\lambda})\right) \qquad (6)$$

where δw is the incremental wall displacement at any distance y below the lowest support, δw_{max} is its maximum value, and λ is the wavelength of the deformation, regarded as proportional to the length s of the wall below the lowest level of current support $\lambda = \alpha s$.

O'Rourke (1993) defined the wavelength of the deformation as the distance from the lowest support level to the fixed base of the wall. Osman and Bolton (2006) suggested a definition for the wavelength of the deformation based on wall end fixity. For walls embedded into a stiff layer beneath the soft clay, such that the wall tip is fully fixed in position and direction, the wavelength was set equal to the wall length (α = 1). For short walls embedded in deep soft clay, the maximum wall displacement occurs at the tip of the wall so the wavelength was taken as twice the projecting wall length (α = 2). Intermediate cases were described as restrained-end walls ($1<\alpha<2$). For the excavation in deep soft clay layer, the α value is found to be 1.3-1.5. It should be noted that this

value would be a function of soil-wall relative stiffness.

The settlement tough occurs at some distance away from the wall, which is slightly different from the triangular tough pattern observed by Powrie (1986). The subsequent stages of excavation involve deep-seated soil flow mechanism and bulging of the retaining wall below the lowest level of struts (Figure 9(b)). The maximum incremental lateral wall displacement for the second and the third stages were 30mm and 90mm (0.5mm and 1.5mm in model scale), respectively. These movements were equivalent to about 0.6% and 1.5% of average incremental engineering shear strain, respectively, within the deformation zone according to Bolton et al. (2008).

These findings once again showed the importance of small strain stiffness of over-consolidated soil on analyzing multi-propped excavation problem. The development of settlement toughs is complicated by the superposition of deep settlement tough near the wall. This observation is consistent with the general observation given by Clough and O'Rourke (1990) that the settlement tough of a multi-propped excavation is bounded by a trapezoidal zone extended up to 2 times the maximum excavation depth. It is also noted that the areas underneath the two curves are roughly equal, consistent with zero volumetric strain in undrained conditions.

Effect of depth to stiff bearing stratum

Mana and Clough (1989) presented parametric studies on the effect of depth to the bearing stratum on maximum lateral wall displacement for fixed base wall. Results showed that movements increase with excavation width and depth to the bearing stratum. The magnitude of lateral wall displacement increases by a factor of 1.5 when the depth to the stiff layer doubles. However, soils are considered to be elastic which implies that the local development of plastic strain is not possible and over-prediction of soil movements.

Jen (1998) investigated into the same issue again with a more sophisticated numerical constitutive model i.e. the MIT-E3 model. Parametric studies on the effect of depth to the hard stratum on lateral wall displacement for excavation using floating wall were carried out. Results show that the depth of end stratum only affects wall deflection below the excavation level, especially the wall toe. On the other hand, shallower clay would have a stronger impact on the distribution of far-field ground settlement. As the location of the rigid base become shallower, the trail of the settlement trough tapers off much more rapidly. The distance for the tapering off is roughly equal to the depth of stiff stratum.

Figure 10 shows the development of wall displacement and ground settlement as excavation in shallow clay (Test 5) progresses. Since the wall toe is not fixed to the base, wall toe rotation and wall bulging movement are the major deformation mode shape. The lateral wall deformation mode shape is very much similar to that of Test 2 except that the length of the bulge is limited to the depth of stiff layer.

The evolution of the soil displacement mechanism is illustrated in Figure 11 for different stages of excavation. The introduction of the first pair of pre-loaded props induces much inward displacement at the wall crest (as shown in Figure 11(a)). The deformation mechanism changed to a free bulging mode which is equivalent to loading a simply supported beam being held vertically. It is the stage that much wall rotation can be developed since there is no moment restraint for props at the wall crest (as shown in Figure 11(b)). After the introduction of the second props, the wall length below the lowest prop is being moment restrained at the prop location. As an effect, not much wall rotation at the lowest prop location could be observed for excavation stage 3 (Figure 11(c)). The maximum lateral wall displacement for the second and the third stages were 45mm and 100mm, respectively. These movements were equivalent to about 0.9% and 2% of average overall engineering shear strain, respectively, within the deformation zone according to Bolton et al. (2008).

The amount of maximum wall displacement is not affected by the depth to the stiff stratum. The difference in the two tests is within 10%. This is comparable to the observation by numerical simulated result by Jen (1998) suggesting that the maximum wall movement would differ only by 20% when the depth of stiff layer increase from 5m to over 50m below wall toe. The settlement profile of the present test does show a much rapid tapering off as the distance get further away from wall. This observation echoes the results simulated by FEA by Jen (1998). This implies that an engineer who wants to control the extent of excavation induced movement should have considered fixing wall toe with ground improvement methods.

Effect of wall toe fixity conditions

For deep excavation in soft ground, the maximum wall deflection of the retaining wall usually occurs at the final excavation level. To limit wall deflection at this level, ground improvement techniques (e.g. Jet-grouting) are usually employed prior to an excavation. A common approach is to improve the entire soil layer within the excavation zone below the excavation level to fix the

wall toe. In the present study, a centrifuge test (Test 3) is carried out to understand how an infinitely stiff fixed base grout layer at the wall toe would affect the deformation mechanism.

Figure 12 shows the variation of wall displacement and ground settlement as an excavation using a fixed based wall (Test 3) progresses. Since the wall toe is fixed to the base, only wall bulging movement is allowed as the deformation mode shape. The lateral wall deformation mode shape is very much similar to that of Test 2 except the fact that a bending moment restraint is being imposed at the wall toe. Figure 12 shows the total deformation mechanism of a fixed base retaining wall for excavation depth of 5.4m. The maximum lateral wall displacement for the second and the third stages were 40mm and 65mm, respectively. These movements were equivalent to about 0.8% and 1.3% of average overall engineering shear strain, respectively, within the deformation zone. In effect, the wall toe fixity restraint controlled lateral soil deformation below final excavation level and the extent of the soil settlement tough away from the wall effectively. A reduction of 50% in lateral wall movement is a result of fixing the wall toe for flexible retaining structures.

Following Clough *et al*.(1989) approach, the incremental wall displacement can be represented by a normalized wall displacement and depth below lowest prop relationship normalized with wavelength of deformation shown in Figure 13. Results show that the normalized curves for both floating and fixed base wall broadly follow the cosine curve. The assumed deformation mode shape is proven to be a good representation of a typical wall bulging displacement profile below the lowest prop for multi-prop deep excavation stages. The wavelength of deformation is a function of depth to the stiff layer. For fixed based wall, the wavelength is the same of the unsupported length of the wall below the lowest prop; whereas the wavelength of the floating wall is equal to 1.3-1.5 times the unsupported length of the wall below the lowest prop. A simplified deformation mechanism for narrow excavation is suggested by Lam and Bolton (2012) as shown in Figure 13. This mechanism of shearing at constant volume consists of three zones of distributed shear and generally represents a continuous and compatible flow of soils with no relative sliding at boundaries. Along the dashed flow lines, the displacement is described by a cosine function in Equation (6).

Effect of wall stiffness

Clough *et al*. (1989) proposed a semi-empirical procedure for estimating movement at excavations

in clay in which the maximum lateral wall movement; δ_{hm} is evaluated relative to factor of safety (FS) and system stiffness, which is defined as follows:

$$\text{System stiffness } (\eta) = EI/\gamma_w h^4. \quad (7)$$

,where EI is the flexure rigidity per unit width of the retaining wall, γ_w the unit weight of water and h the average support spacing.

The variation of maximum normalized measured lateral displacement (w_{max}/H) with system stiffness (η) as defined in Equation (8) is shown in Figure 15. A worldwide database of excavation cases in soft clays (c_u <75kPa) as reported in Lam and Bolton (2012) is also included for reference. Lam and Bolton (2012) showed that the normalized lateral wall displacement decreases with increasing FS generally. However, there is no simple dependence of normalized wall displacement on FS. Similar observations were made from the centrifuge experimental data. The measured data with similar FS and system stiffness in the same stage of excavation scatters in a wide range. It could be due to the fact that the use of factor of safety to quantify wall deformation ignores small strain non-linear stiffness of the soil, the incremental nature of the construction and most importantly size of the deformation mechanism.

Effect of soft props response

According to Jen (1998), reductions in strut stiffness case increases in the wall deflection occurring above the excavation grade with the maximum wall deflection occurring closer to the excavated level whereas the lateral soil movement below the excavation level is not influenced by the stiffness of the prop system. As the props become more compressible, the maximum wall movement increases with negligible movement of the settlement tough position. The reduction of prop stiffness also causes the soil to develop a shallower failure mechanism. A centrifuge experiment Test 4 was carried out to investigate the issue. The prop stiffness is obtained by conducting axial-load displacement tests in a loading rig. The target stiffness of a fully-saturated prop is found to be about 1660N/mm in model scale. For the present test, the prop stiffness is adjusted to be 550N/mm in model scale. Figure 16 shows the development of wall deformation and ground settlement with progress of excavation. The lateral wall deformation mode shape is very much similar to that of Test 1 except the fact that soft prop response allows rigid body displacement of the retaining wall into the excavation pit. Figure 16 shows the total deformation mechanism of the test. Triangular wedge mechanism (45 degree shear planes) is found to be the

major mechanism on the active side. The maximum lateral wall displacement for the second and the third stages were 37mm and 80mm, respectively. These movements were equivalent to about 0.74% and 1.6% of average overall engineering shear strain, respectively, within the deformation zone. Since soft response of the props allows rigid body lateral displacement of the wall, soil on the active side is being sheared at an angle 45 degree. A spandrel type settlement profile with the same width of the length of the wall is induced. This extra soil strain developed on the active side may have induced strain dependent degradation of soil stiffness causing more soil deformation as the excavation depth goes deep.

Soil strains

This section presents the profiles of engineering shear strain distributions within the soil during the excavation process. Strains are calculated based on the PIV displacements presented in the previous section. A co-rotational deformation formulation is used allowing rotation, translation and distortion, thereby eliminating numerical instability associated with small gauge length, and separating rigid body rotation from deformation (White, 2002).

Strains can be visualized using the Mohr circle of strain as shown in Figure 17. Since the PIV displacement data was obtained from two different cameras, it is difficult to obtain a complete strain profile directly from the PIV method suggested by White *et al*. (2003). A new mesh for soil patches has to be built and the displacement data of the patches needs to be obtained by the linear interpolations. By applying the small strain formulation, all necessary strain components (ε_{xx}, ε_{zz},ε_{xz}) can be obtained and used to obtain engineering shear strains.

The calculation of strain is highly vulnerable to errors in PIV displacement data. Errors evolve as a result of the level of accuracy of PIV data considering very small movement and more obviously from the difficulties associated with stitching PIV data from different pictures together. The standard deviation in pixel space for the present calibration procedure is about 0.3 pixels which correspond to 0.1mm error in model scale (or 6mm in prototype scale at 60g).

Engineering shear strain calculation

The engineering shear strain is a useful quantity to understand the mechanism by which interaction between the retaining structure and the soil can be addressed. For plane-strain conditions, shear strain, ε_{xz}, and the engineering shear strain, γ, can be visualized using the Mohr circle of strain. The engineering shear strain can be calculated using the following equation:

$$\gamma = \sqrt{(\varepsilon_{xx} - \varepsilon_{zz})^2 + (2\varepsilon_{xz})^2} \quad (8)$$

Figure 18 (a), (b) and (c) show the engineering shear strain map on the active side for excavation depths of 1.08m, 3.24m and 5.40m, respectively for Test 5.

For an excavation depth of 1.08m, the wall behaved as a simple cantilever; then the first layer of props was introduced, and slightly pre-loaded. Due to the increase in lateral stress near the soil surface, some shear strain concentration happened near the wall crest on the retained side.

When the excavation depth had increased to 3.24m, the 2nd layer of props was introduced. A shear zone developed near the wall toe as a result of wall rotation about the crest of the retaining wall. The average shear strain level was the about 1%.

After installation of the third layer of props, any further movement must be deep-seated. Clearly, a deep seat soil movement developed. A shear band developed from the wall toe and extended upwards towards the soil surface. It is interesting that the width of the shear band develops as it extends above the elevation of the lowest prop towards the soil surface, alongside a zone with smaller shear strain next to the retaining wall above the lowest prop.

Data of the cases from Test 1 (Figure 18c) and Test 2 (Figure 18d) offer the opportunity of examining the difference in mechanism when comparing with excavation cases with a rigid wall and a flexible wall. Due to the rigidity of the retaining wall, wall flexure below the lowest prop location is the main deformation mechanism (Test 1). A very thin shear band developed at the toe of the wall and extended towards the soil surface. In contrast to the behaviour of soil around a flexible wall, no soil arch forms as a result of the rigidity of the displacement boundary which suppresses bulging of the wall.

Validation of the energy conservation principle

A simple analytical design framework, namely Mobilizable Strength Method (MSD), was introduced by the principle of conservation of energy within a geo-structural mechanism by Lam and Bolton (2012). A typical bulging displacement for each excavation stage was calculated by considering an admissible deformation mechanism for base heave. The mobilizable shear strength was deduced from the mechanism, by conservation of energy. The work done by shearing of the soils was said to balance the potential energy change of soil within and the structural energy stored in the system for each excavation increment. This incremental approach provides a simple tool for

deformation assessments. The following analysis validates this design methodology using experimental evidences.

By conservation of energy of a geo-structural mechanism (Lam and Bolton, 2012), the total loss of potential energy of the soil (ΔP) must balance the total work done in shearing the soil (ΔW) and the total elastic strain energy stored in bending the wall (ΔU_1) and in compressing the props (ΔU_2).

$$\Delta P = \Delta W + \Delta U_1 + \Delta U_2 \tag{9}$$

The potential energy loss on the active side of the wall and the potential energy gain of soil on the passive side can be calculated easily. The net change of gravitational potential energy (ΔP) is given by the sum of the potential energy changes for each soil patch:

$$\Delta P = \sum_{i=1}^{n} \left[\int_{Area} \gamma_{sat}(i) dw_y(i) dA \right] \tag{10}$$

,where $\delta w_y(i)$ is the vertical component of displacement of soil in the i^{th} soil patch; $\gamma_{sat}(i)$ is the saturated unit weight of soil in the i^{th} soil patch.

While calculating the engineering shear strain, soil elements are formed as triangles linking three neighboring patches. The total work done ΔW in shearing the soil is given by summing for each element:

$$\Delta W = \sum_{i=1}^{n} \left[\int_{Area} c_{mob}(i) |\delta\gamma(i)| dA \right] \tag{11}$$

,where $c_u(i)$ is the undrained shear strength of soil in the ith element; $d\gamma(i)$ is the shear strain increment of soil in the ith element; and the corresponding mobilized strength ratio is given by the stress-strain relation defined by the simple power law derived from Equation (4) and (5).

$$\frac{c_{mob}}{c_u} = \left(\gamma / \gamma_u \right)^a \tag{12}$$

,where the γ_u and a parameters are found to be 5% and 0.33. The work done per unit area in the element is basically calculated as the area under the stress strain curve.

The total elastic strain energy stored in the wall, ΔU_1, can be evaluated by repeatedly updating the deflected shape of the wall. It is necessary to do this since U is a quadratic function of displacement.

$$\Delta U_1 = \int_0^s \frac{EI\kappa^2}{2} dx = \int_0^s \frac{M^2}{2EI} dx \quad (13)$$

,where E and I are the elastic modulus and the second moment of area per unit length of wall, and s is the length of the wall below the lowest prop.

The total elastic energy stored in the props, ΔU_2, can be estimated by calculating the sum of the product of the displacement of prop after installation and the maximum prop force at different elevations.

$$\Delta U_2 = \sum_{i=1}^{n} \frac{F_i w_i}{2} \quad (14)$$

,where F_i is the maximum prop force after installation and w_i is the corresponding compressive displacement.

Following the strain map created by the PIV data, a work map is calculated. Figure 19 shows the total work done per meter at model scale by the soil around an excavation in shallow clay using a flexible wall (Test 5) at different stages of excavation. The total work done at different stages is calculated by Equation 11. On the other hand, the total potential energy change by the soil elements at different stages is evaluated by Equation 10 and the distribution is plotted in Figure 20. The wall bending elastic energy and the prop compressive elastic energy are examined by Equation 13 and 14, respectively. Ideally, the potential energy change (ΔP) should be equal to the sum of work done by shearing of the soil, the elastic energy stored in the retaining structure ($\Delta U_1+\Delta U_2+\Delta W$) assuming minimal boundary friction at interfaces of solid boundaries and soil. Except for the first excavation stage of Test 5, the calculated potential energy change is within 25% of the calculated work done on the soil structure system. For the first excavation stage, since fine measurements of displacement from the PIV data is prone to error due to control markers calibration and photo stitching, the difference between ΔP and $\Delta U_1+\Delta U_2+\Delta W$ is as large as 64%. The variation of the potential energy change and work done by the soil structure system is plotted on Figure 21. The difference of the energy terms is less than 30%. Table 2 summarizes the results of the studies of Test 2, Test 3 and Test 5. Results suggested that the ΔP and $\Delta U_1+\Delta U_2+\Delta W$ agree well generally.

Following the analytical procedures described in Lam and Bolton (2012), prediction of lateral wall

displacement profiles for centrifuge Test 1 and Test 2 could be compared with the observations in Figure 22. The calculations adapts the same undrained strength profiles with appropriate construction sequences, geometries of structures and excavation and small-strain stress strain relationships as described earlier in the paper. The displacement profile typically fell within 30% of the observation in the centrifuge. Similar validation of the method carried out in Lam and Bolton (2012) shows predictions within an error of 40% for more than 100 field records. Considering the lack of any detailed account of the soil anisotropy, the performance of the MSD prediction is satisfactory.

Table 2 A summary of calculated energy terms for different tests

Test & stage		ΔU_1(J/m)	ΔU_2(J/m)	ΔW(J/m)	$\Delta W+ \Delta U_1 +\Delta U_2$(J/m)	ΔP(J/m)	% error
Test 5	1	0.007	0.03	2.3	2.3	1.1	-52.9
	2	0.98	0.08	3.1	4.2	3.2	-23.1
	3	1.1	0.19	12.8	14.1	14.3	1.49
Test 3	1	0.006	0.08	3.3	3.4	2.5	-34.2
	2	1	0.12	7.4	8.5	6.9	-23.4
	3	0.1	0.17	24.5	24.8	21.6	-12.8
Test 2	1	0.007	0.09	2.5	2.6	1.6	-63.5
	2	1.00	0.12	3.3	4.4	3.9	-12.8
	3	2.4	0.16	12.5	15.1	14.9	-1.06

Conclusions

With the aid of an advanced physical model and proper instrumentations, the performance of various model excavations was monitored. Observed ground deformation was closely monitored during the centrifuge in-flight excavation process. Short term undrained excavation behaviour is ensured by finishing excavation in 40 minutes. Some of the key conclusions are listed as follows:

- During excavation, negative excessive pore water pressure due to vertical unloading is cancelled out by positive excess pore water pressure due to undrained shearing.
- Incremental wall deformation profile generally follows O'Rourke (1993) cosine bulge equation. New deformation mechanisms can be considered by simplifying the observed mechanism with respect with governing parameters such as wall toe fixity condition and excavation geometry. Averaged soil strains mobilized in the system are below 2%, reiterating the importance of small strain stiffness for excavation problem.
- Clough et al. (1989) trend lines for estimating wall lateral displacement in relation to factor of safety generally applies to observed data. Should improvement on accuracies of

the approach be considered, engineers may look into small strain stiffness of soils, incremental construction sequence and most importantly the characteristics of the deformation mechanisms.

- In general, the change in maximum wall displacement is sensitive to the fixity at the wall toe instead of the depth of the clay stratum. The extent of the settlement profiles, however, is a function of the depth of the clay stratum. A tapering off trend was observed as a result of the limited size of a deformation mechanism by the depth of the layer.
- Reduction of strut stiffness increases the wall deflection above the foundation level. The softer prop response effectively induced a much shallower and local triangular mechanism with deep and narrow tough developed near the retaining structures.
- Computed engineering shear strains shows premature shear band developed at the toe of the rigid wall case, whereas wider shear zone developed between the wall toe and the lowest propping location and then extended upwards towards soil surface with a neighboring stagnant zone at shallow depths near the wall.
- The conservation of energy as a principle for mobilizable strength design method is validated with experimental evidences satisfactorily. The performance of the method prediction fells within 30% of the measurements.

A relatively simple MSD analysis could be performed within a reasonably short time period for designers, which could be a useful tool in taking key design decision as a precursor of a site-specific numerical analysis.

REFERENCES

Bolton, M. D., Lam, S.Y. and Osman, A.S. (2008). Supporting excavations in clay-from analysis to decision-making. Special Lecture, *6th International Symposium of Geotechnical Aspects of Underground Construction in Soft Ground.* April, Shanghai.

Clough, G.W. and O'Rourke, T. D., (1990). Construction induced movements of in situ walls. In *Proc. Design and performance of earth retaining structure*, ASCE Special conference, Ithaca, New York, pp439-470.

Clough, G.W. and Smith, E. W. and Sweeney, B. P.(1989) Movement control of excavation support system by iterative design. *Foundation Engineering Current Principles and Practices*, Vol.2 ASCE, New York, NY, 1989, pp.869-882.

Jen, L. C. (1998). The design and performance of deep excavation in clay. *Ph.D thesis*, MIT.

Lam, S.Y. and Bolton, M.D. (2012). Energy conservation as a principle underlying mobilizable strength design for deep excavations. *Journal of Geotechnical and Geoenvironmental Engineering, ASCE*, Vol.137, pp.1062-1075.

Lam, S.Y., Elshafie, M.Z.E.B., Haigh, S.K. and Bolton, M.D. (2012). Development of a new apparatus for modeling deep excavation related problems in geotechnical centrifuge. *Journal of physical modeling in geomechanic*, Vol. 12, Issue 1, March, 2012, pp24-38.

Leong, E.C., Yeo, S.H. and Rahardjo, H. (2005). Measuring shear wave velocity using bender elements. *Geotechnical Testing Journal*, Vol. 28, no.5, pp.488-498.

Jamiolkowski, M., Ladd, C.C., Germaine, J.T., and Lancellotta, R. (1985). New developments in field and laboratory testing of soils. Proc. of 11th *ICSMFE*. Vol.1, 1985, pp57-153.

Madabhushi, S.P.G., Houghton N.E., and Haigh S.K. (2006). A new automatic sand pourer for model preparation at University of Cambridge. Proc. *ICPMG'2006*, Hong Kong, pp 217-222.

Mana, A. I. and Clough, G. W. (1981). Prediction of movements for braced cuts in clay. ASCE *Soil Mechanics and Foundations Division Journal*, 107(6): 759-777.

Osman, A. S. & Bolton, M. D. (2004). A new design method for retaining walls in clay, *Canadian Geotechnical Journal*, 41(3): 453-469.

Osman, A. S. and Bolton, M. D. (2006). Ground movement predictions for braced excavations in undrained clay. *J. Geotech. & Geoenvir. Engrg.*, ASCE, Vol. 132, No. 4, April 1, 2006.

O'Rourke, T.D. (1993). Base stability and ground movement prediction for excavations in soft clay. *Retaining structures*, Thomas Telford, London, 131-139.

Powrie, W. (1986). The behaviour of diaphragm walls in clay *Phd thesis*, University of Cambridge.

Vardanega, P.J. (2012). Strength mobilization for geotechnical design and its application to bored piles. *PhD. Thesis*, University of Camrbidge.

White, D.J. & Take, W.A. (2002). GeoPIV: Particle image velocimetry(PIV) software for use in geotechnical testing, *Technical Report CUED/D-SOILS/TR322*, October 2002, University of Cambridge.

White, D.J. Take, W.A. and Bolton M.D. (2003). Soil deformation measurement using Particle Image Velocimetry (PIV) and Photogrammetry. *Geotechnique* 53(7): 619-631.

Zhao, Y., Gafar, K., Elshafie, M.Z.E.B., Deeks, A.D., Knappett, J.A. & Madabhushi, S.P.G. (2006). Calibration and use of a new automatic sand pourer. Proc. of *ICPMG 2006*, pp265-270.

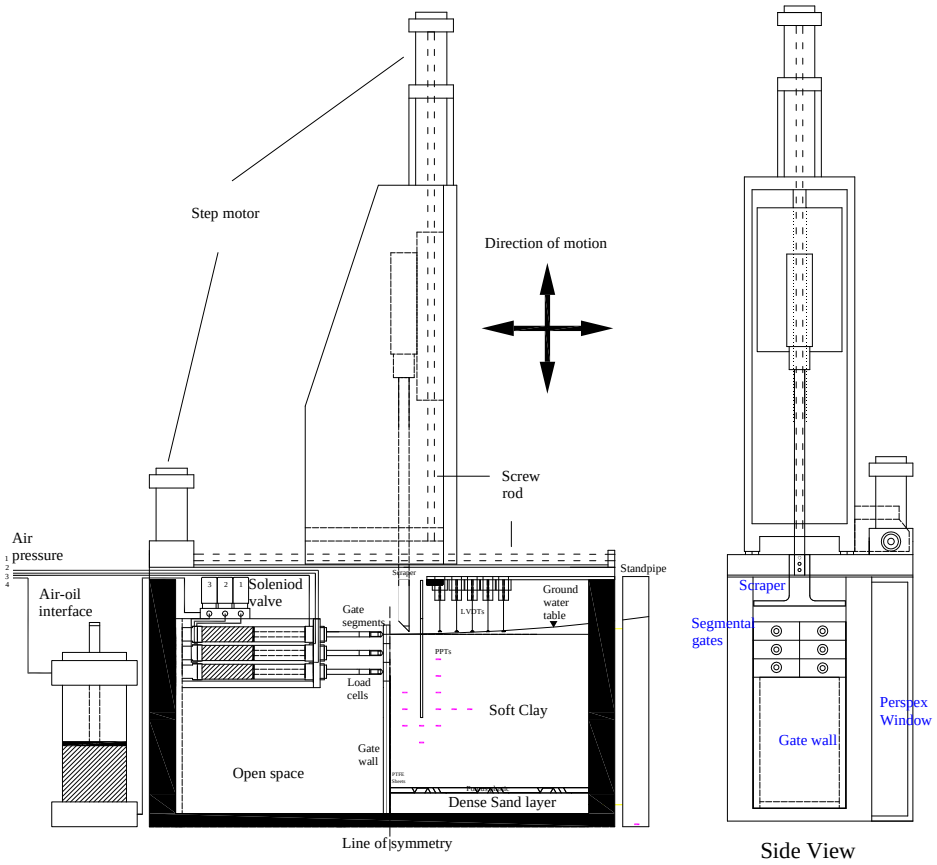

Figure 1 Schematic diagram of experimental setup with in-flight excavator

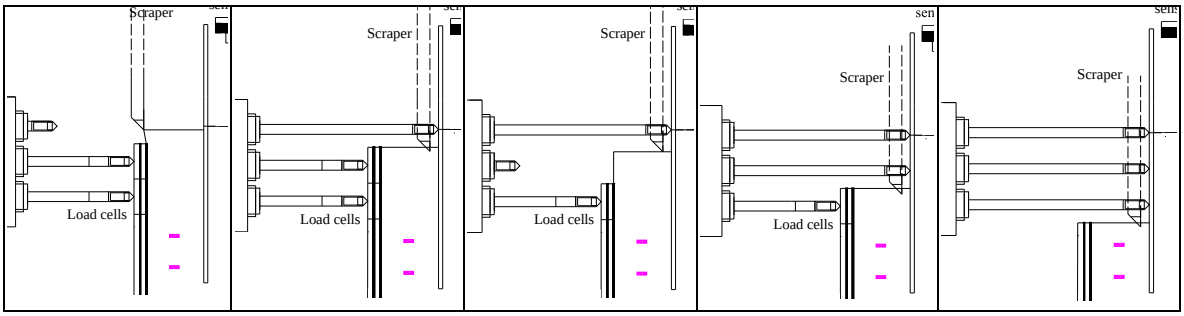

Figure 2 Modeling sequences of excavation

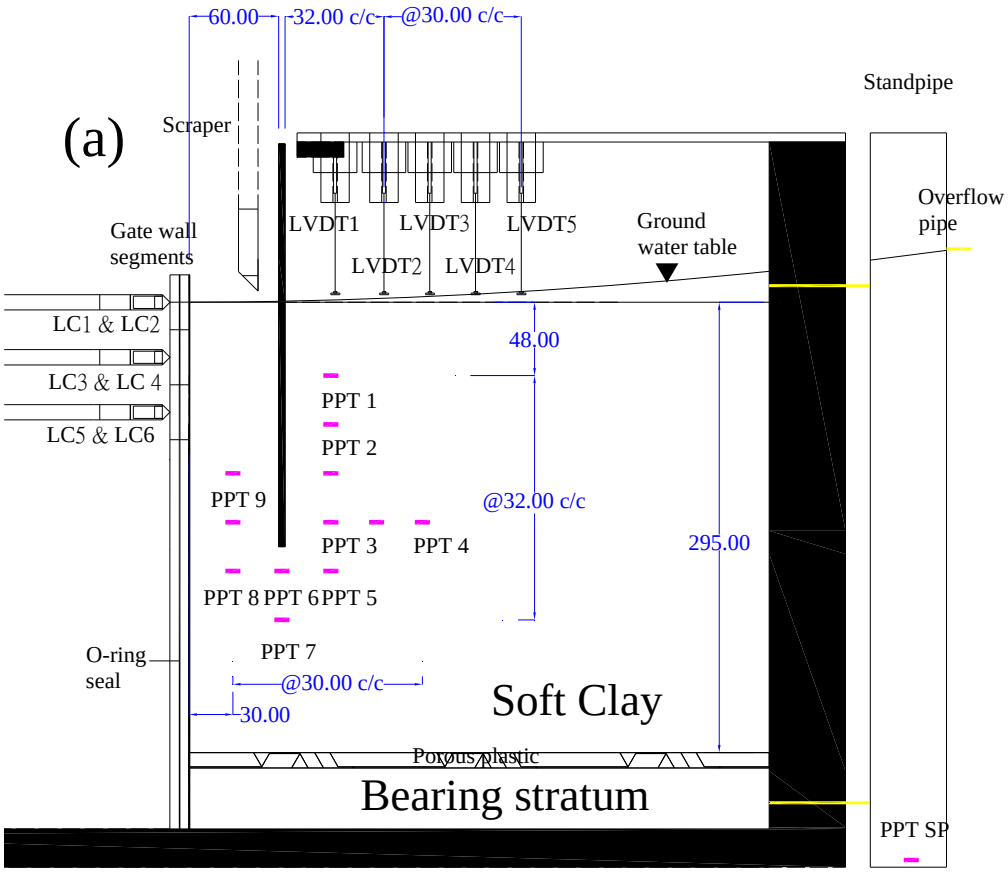

Figure 3 Positions of instruments on model package in elevation view (in mm)

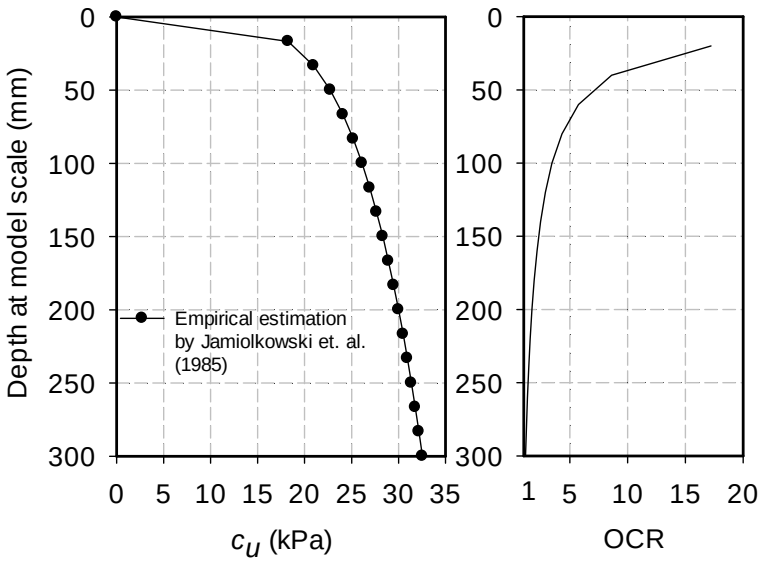

Figure 4 Undrained shear strength and over-consolidation profile at 60g

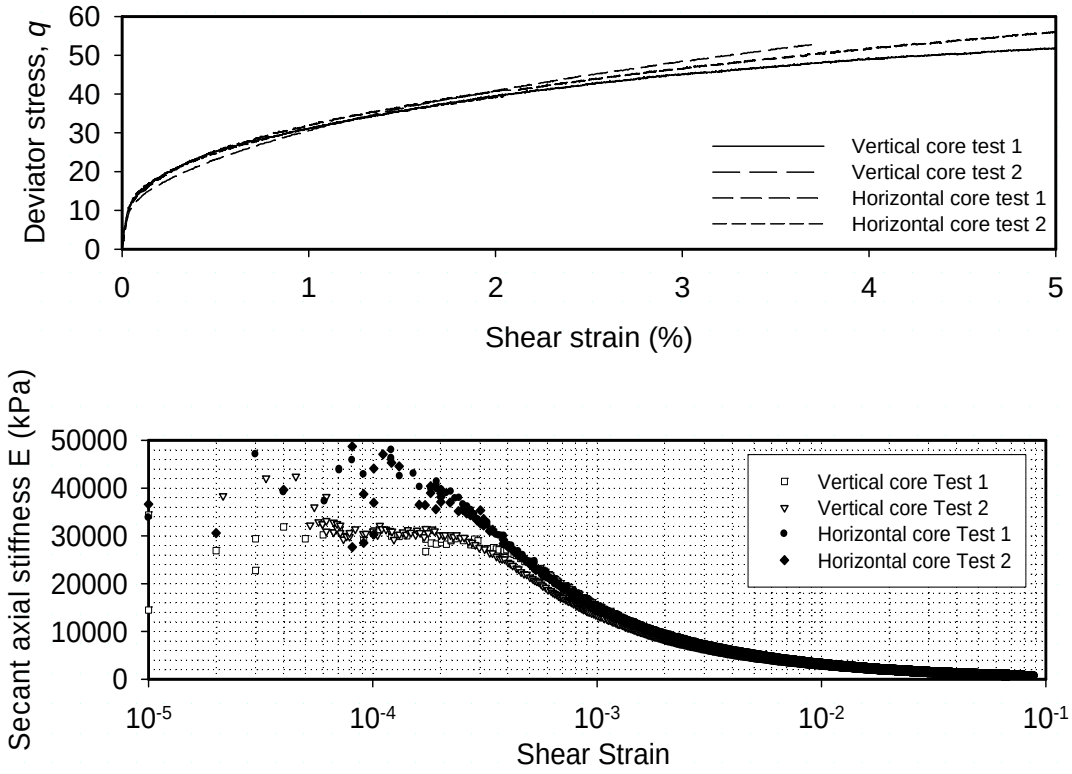

Figure 5 Stress strain curves and stiffness degradation curves for vertical and horizontal core sample.

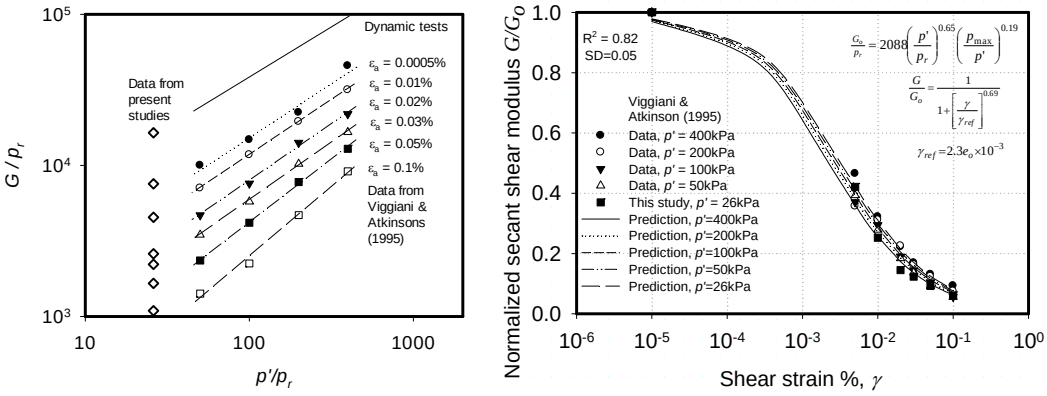

Figure 6 Variation of measured and predicted shear modulus (G) with mean stress and shear strain from triaxial tests in (a) G/p_r vs p'/p_r space and (b) G/G_o vs γ space

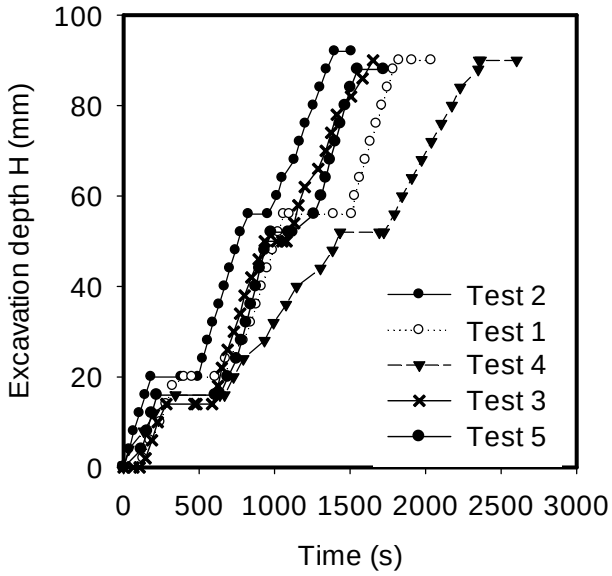

Figure 7 Progress of excavations

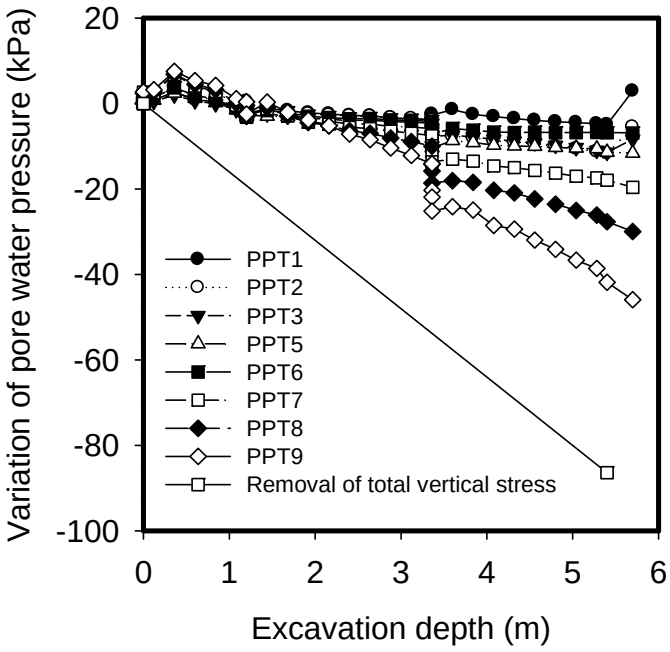

Figure 8 Variation of excess pore water pressure during excavation with stiff props and wall (Test 1)

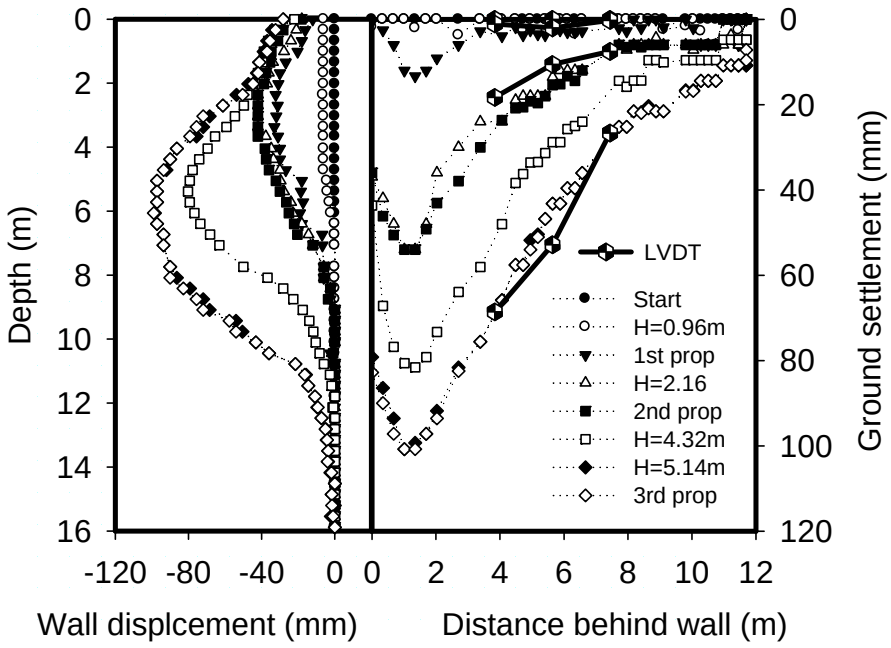

Figure 9 Development of wall deformation and ground settlement with progress of excavation (Test 2).

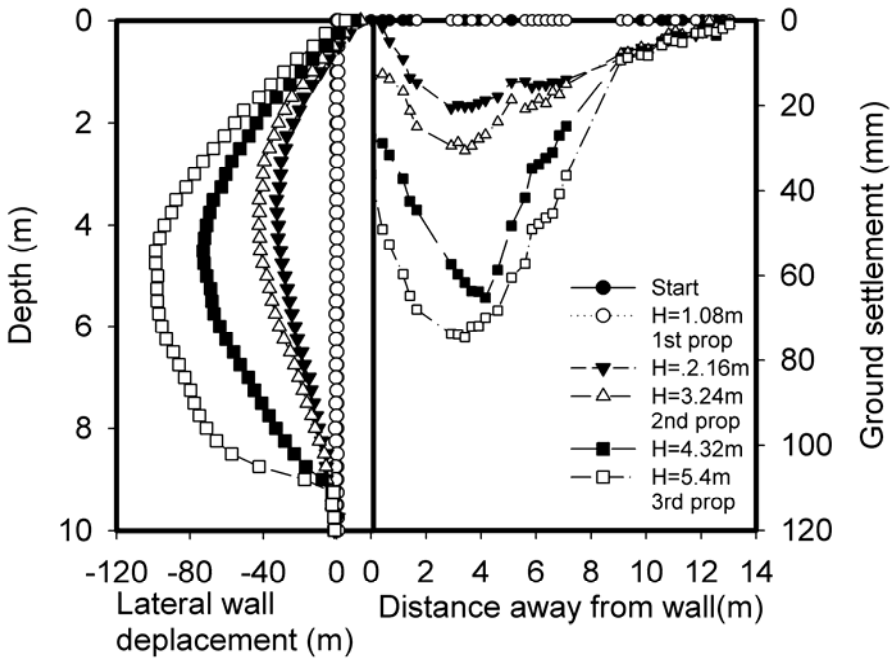

Figure 10 Development of wall deformation and ground settlement with progress of excavation (Test 5)

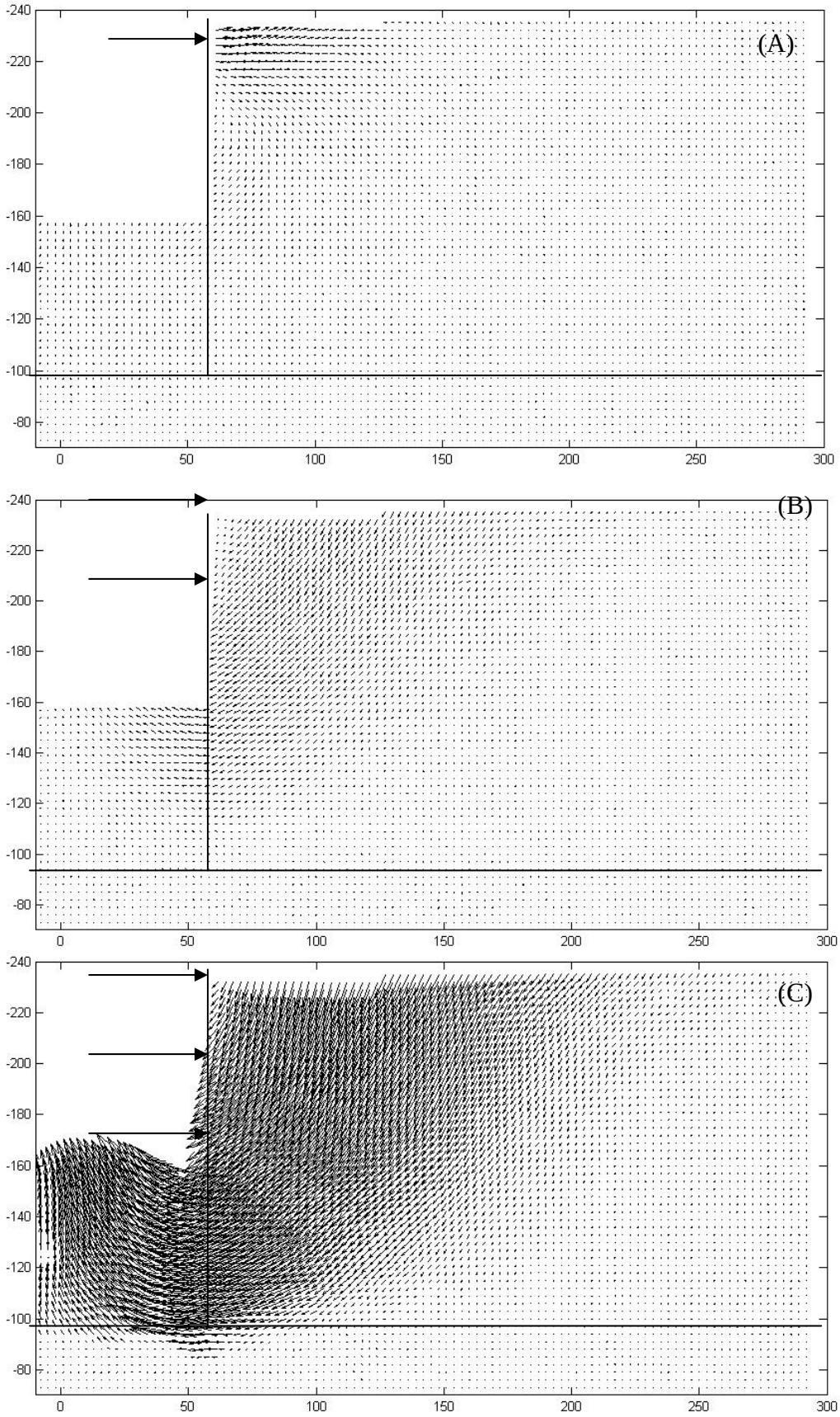

Figure 11 Incremental displacements for different stage of excavation for Test 5

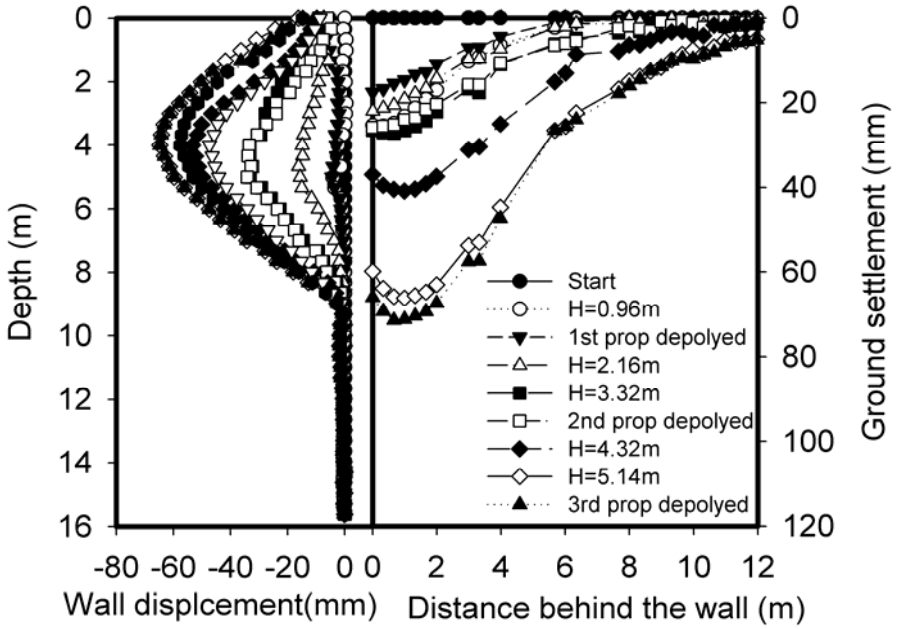

Figure 12 Development of wall deformation and ground settlement with progress of excavation (Test 3).

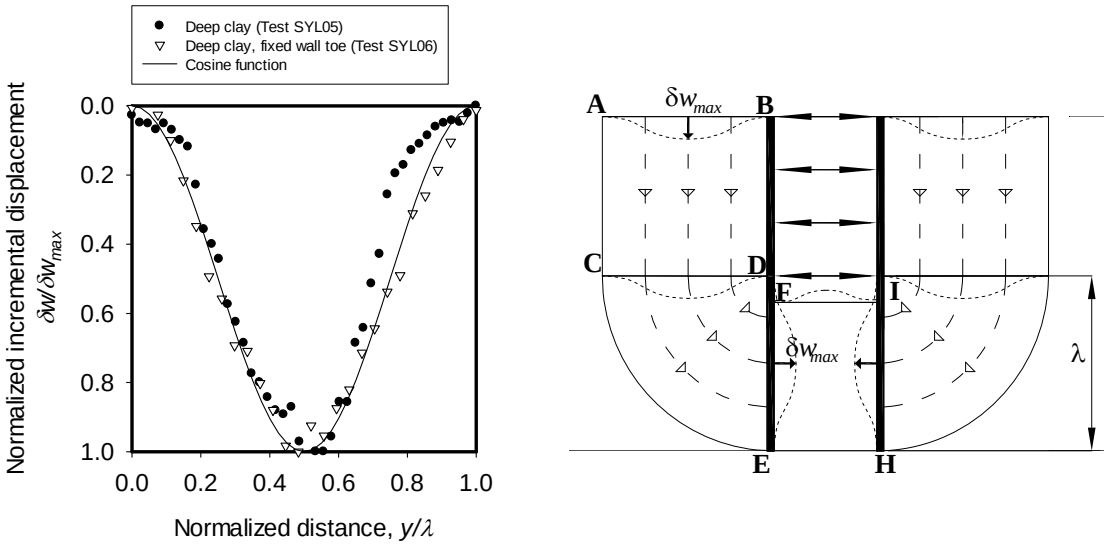

Figure 13 Variation of normalized incremental displacement with distance below the lowest prop and simplified deformation mechanism

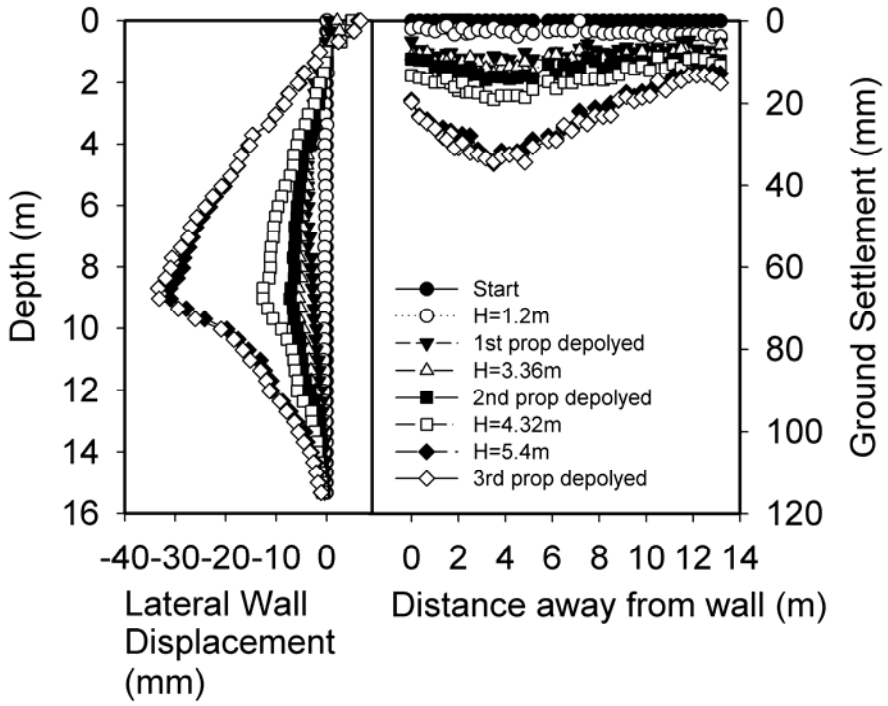

Figure 14 Development of wall deformation and ground settlement with progress of excavation (Test 1)

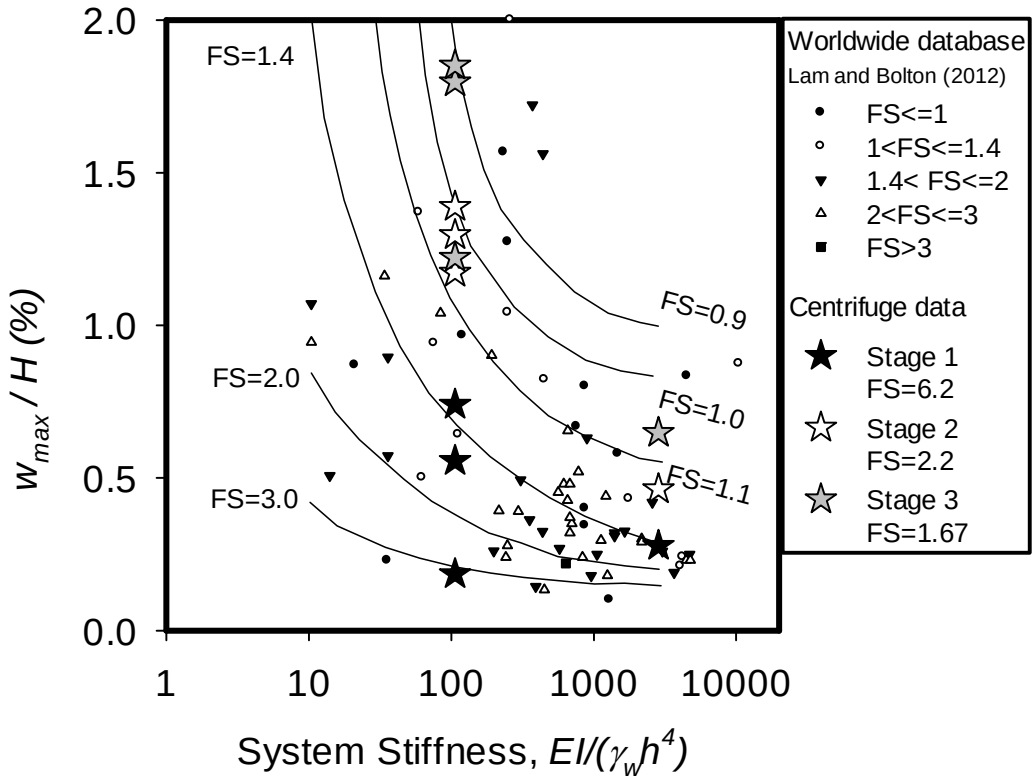

Figure 15 Variation of maximum horizontal wall displacement with System stiffness defined by Clough et al. (1989) and factor of safety against base heave.

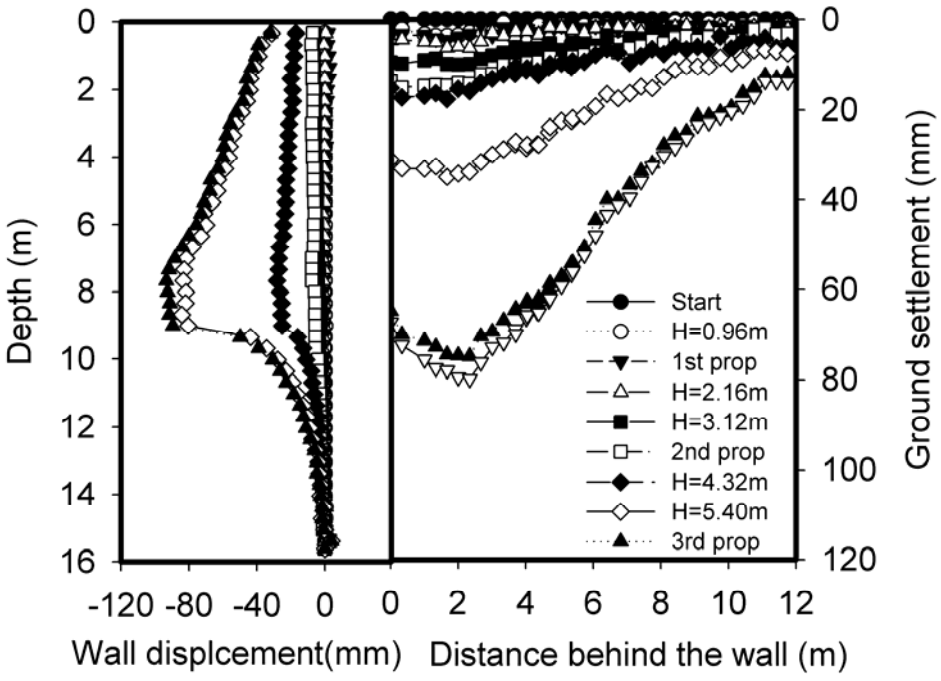

Figure 16 Development of wall deformation and ground settlement with progress of excavation (Test 4).

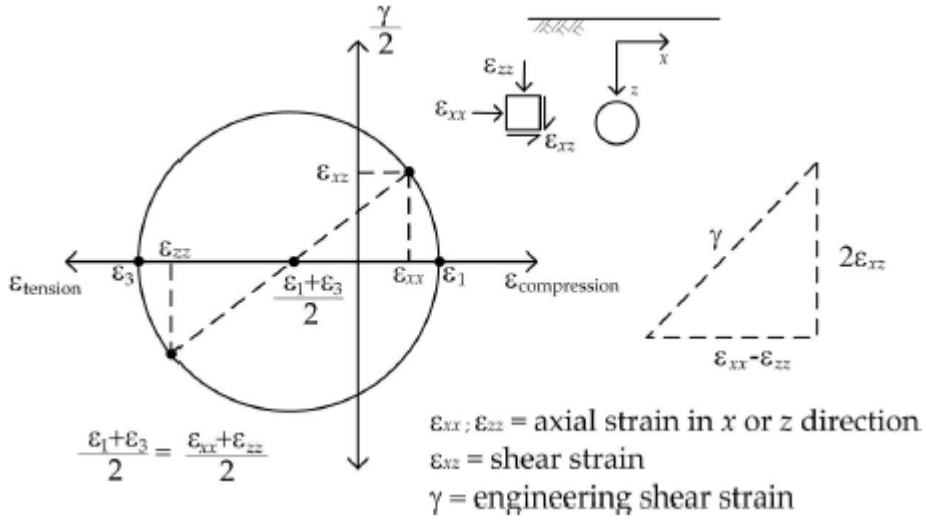

Figure 17 Mohr circle of strain

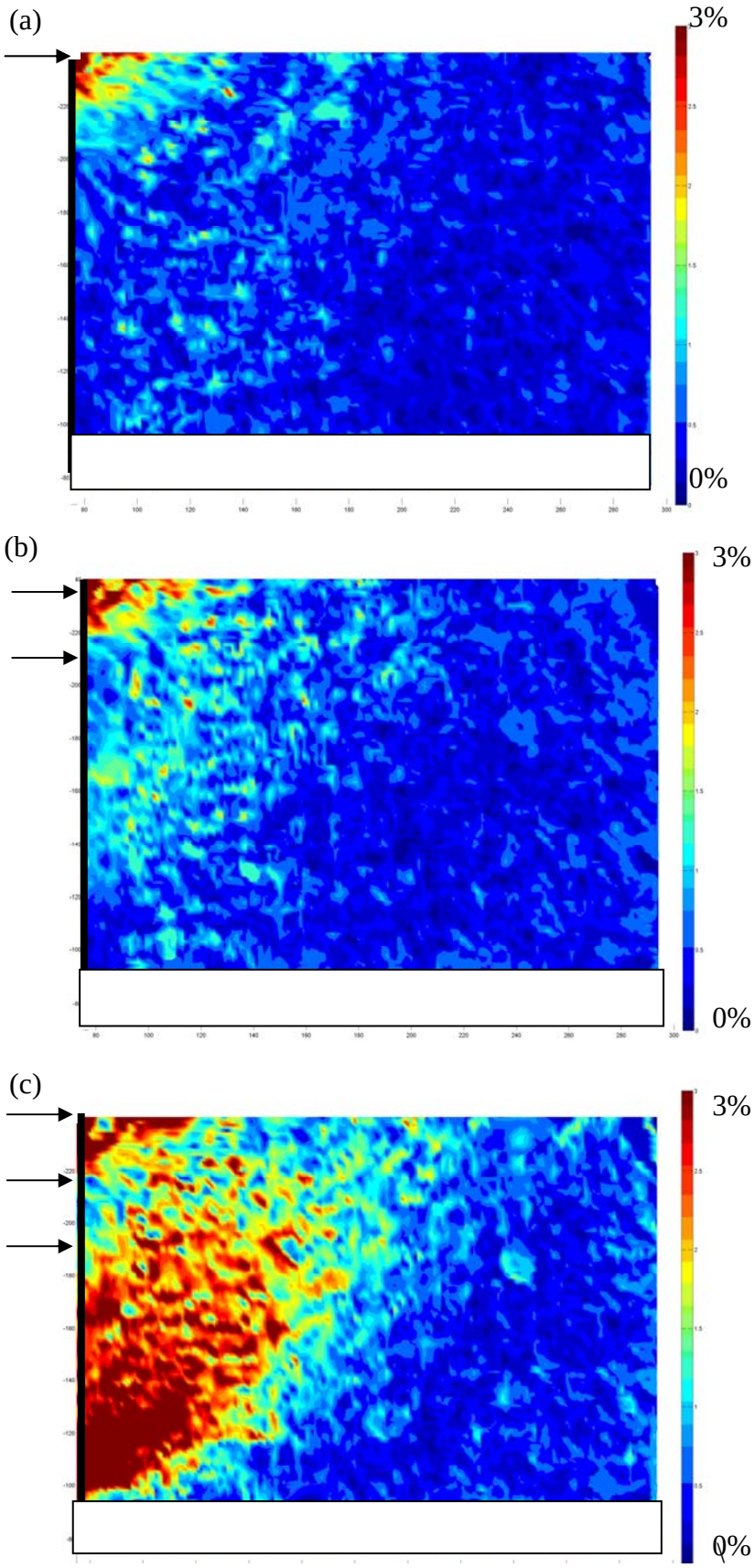
(a)
3%
0%
(b)
3%
0%
(c)
3%
0%

(d)

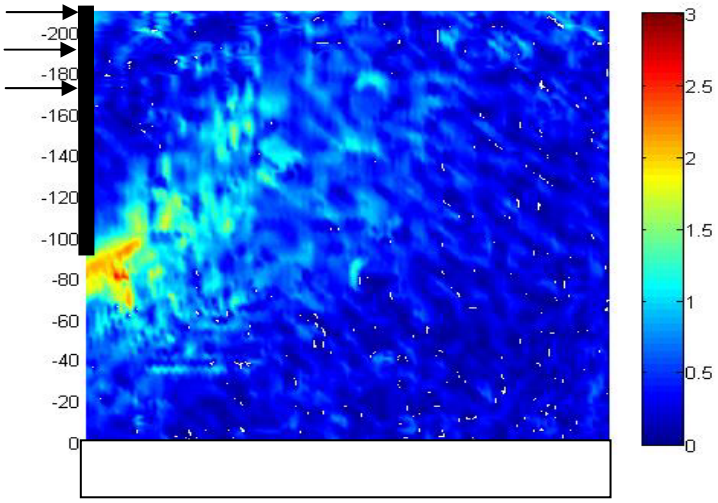

Figure 18 Engineering shear strain plots on active side for Excavation depth of (a) Stage 1, (b) Stage 2 and (c) Stage 3 for Test 5 and (d) Stage 3 for Test 1

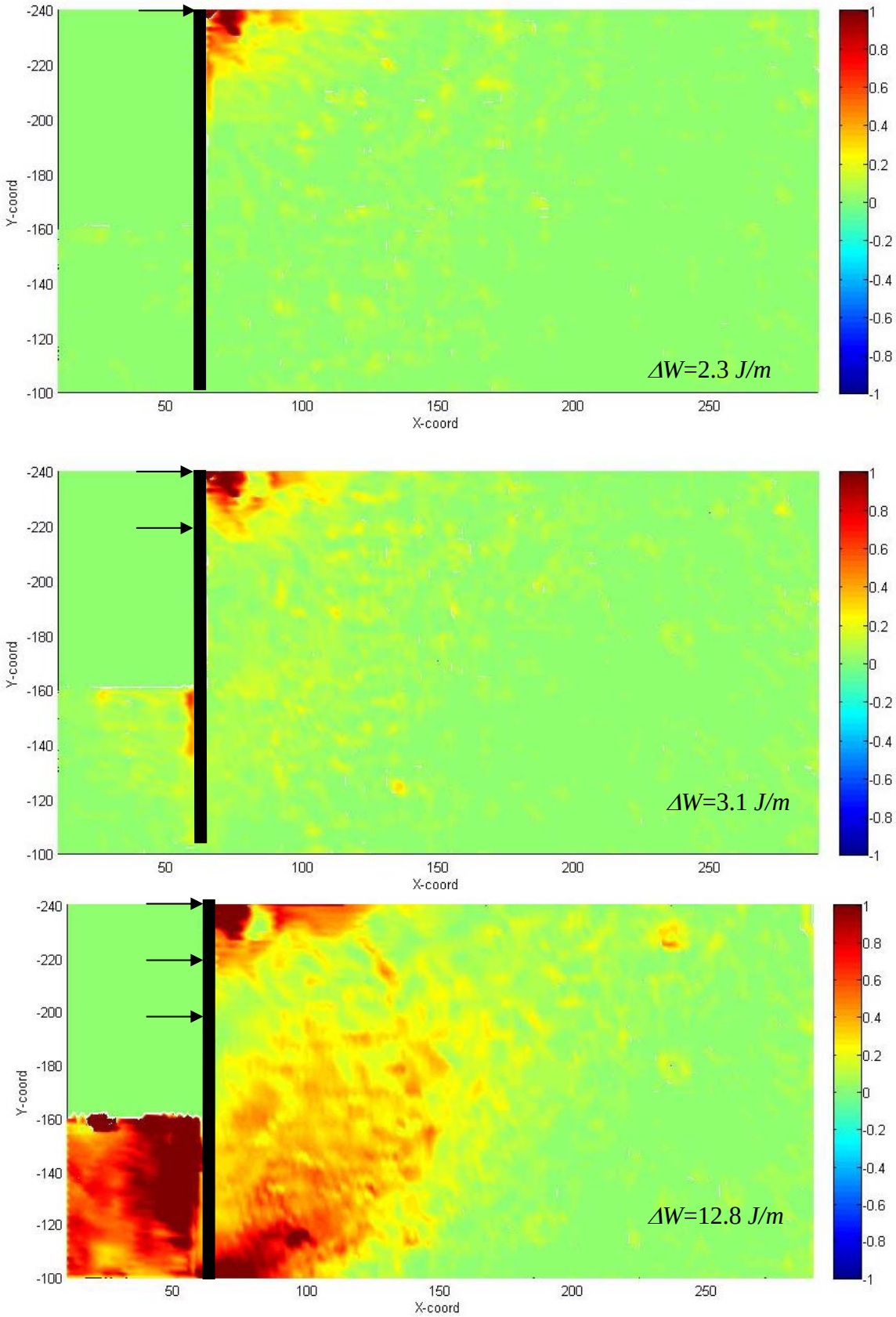

Figure 19 Work done in excavation depth of 1.08m, 3.24m and 5.40m for Test 5

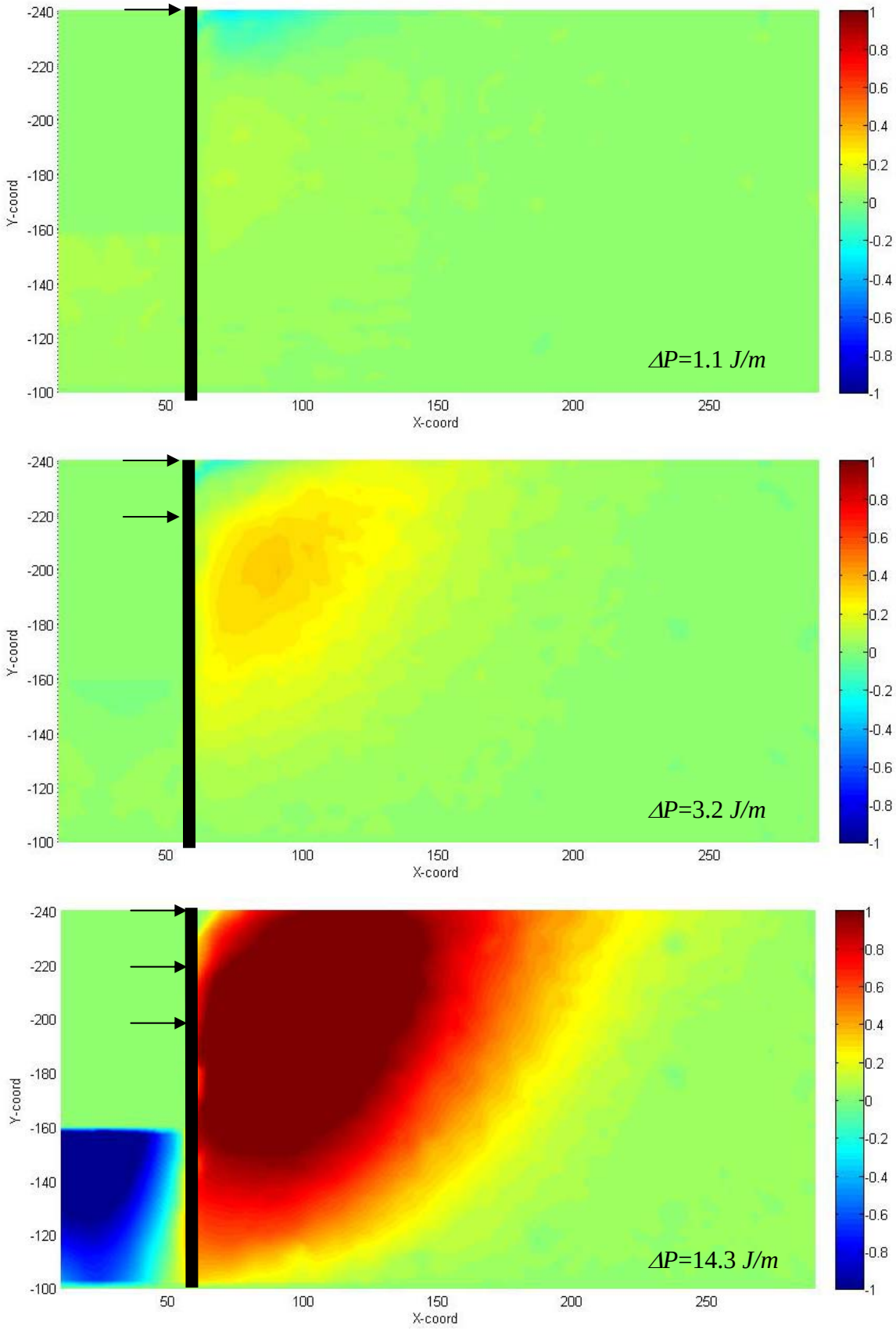

Figure 20 Potential energy change for excavation depth of 1.08m, 3.24m and 5.40m for Test 5

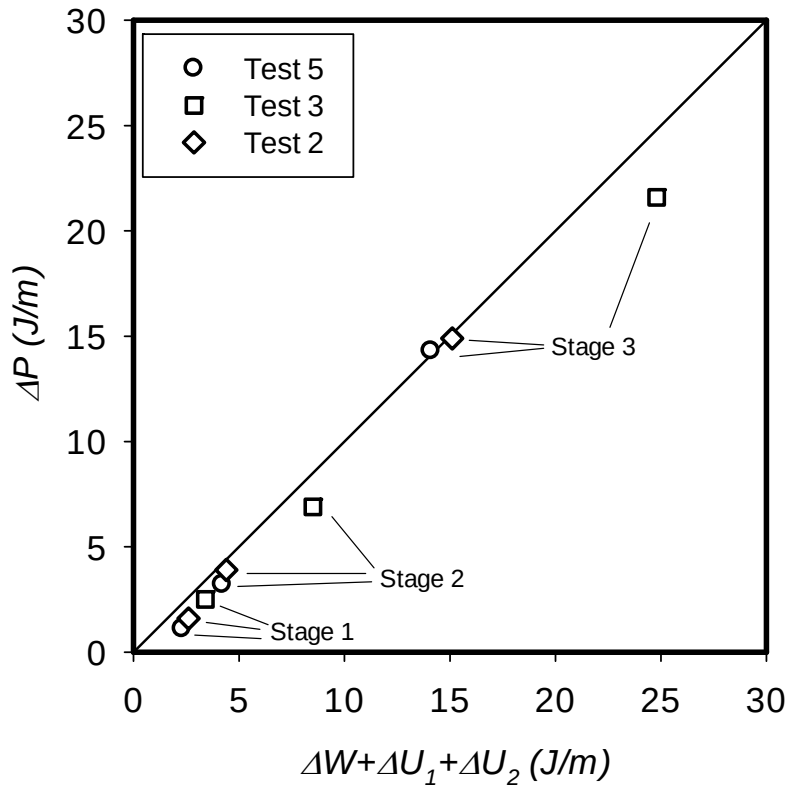

Figure 21 Variation of potential energy change with work done by the soil structural system

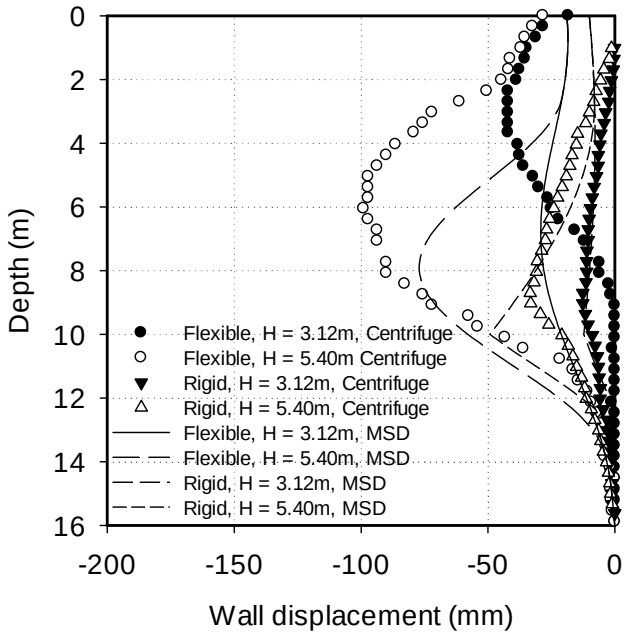

Figure 22 Predicted and measured lateral wall displacement with depths.